R. & M. No. 3014
(16,815)
A.R.C. Technical Report

MINISTRY OF SUPPLY

AERONAUTICAL RESEARCH COUNCIL
REPORTS AND MEMORANDA

Flight Tests on a *Vampire* Mk. 5 With a Redesigned Anti-Snaking Rudder

By
W. J. G. PINSKER

LONDON : HER MAJESTY'S STATIONERY OFFICE
1957
FIVE SHILLINGS NET

Flight Tests on a *Vampire* Mk. 5 With a Redesigned Anti-Snaking Rudder

By

W. J. G. PINSKER

COMMUNICATED BY THE DIRECTOR-GENERAL OF SCIENTIFIC RESEARCH (AIR)
MINISTRY OF SUPPLY

Reports and Memoranda No. 3014*

January, 1954

Summary.—A specially designed rudder has been fitted to a *Vampire* Mk. 5 to act as an aerodynamic yaw damper. Flight tests show that the damping of the lateral oscillation has been substantially increased in consequence a logarithmic decrement greater than unity being attained even at 40,000 ft altitude.

This is a considerable improvement on the results obtained previously on the same aircraft, when the standard rudder was used as the damping surface.

Air to air aiming is shown to have benefited from the effect of the damping rudder.

1. *Introduction.*—It has been shown in Ref. 1 that the damping of the lateral oscillation of an aircraft can be substantially improved by the trailing motion of a rudder, if this has strongly positive floating characteristics ($b_1/b_2 \gg 0$) and is suitably restrained in its movement by a dashpot.

During an earlier series of flight tests the starboard rudder of a *Vampire* Mk. 5 was adapted for this purpose. The damping of the lateral oscillation of the standard aircraft, with the damping rudder locked, is presented in Fig. 1. The corresponding values for the period of the oscillation are given in Fig. 2. When the damping rudder was operating, the logarithmic decrement of the lateral oscillation was increased as plotted in Fig. 3.

This improvement in damping was less than would be expected if the aerodynamic characteristics of the rudder had been more favourable for its role as a damping surface, *i.e.*, if it had had more positive b_1/b_2. In particular, this rudder suffered from a progressive reduction in $(-b_1)$ at the higher Mach numbers. This effect was attributed chiefly to the relatively large trailing-edge angle ($\simeq$ 15 deg).

In order to realize the full potentialities of the damping rudder, a new control surface was designed and built to replace the standard starboard rudder. This control had an increased chord to enable the trailing-edge angle to be reduced and was fitted with a geared tab to reduce the b_2 of the otherwise practically unbalanced surface.

Originally it was intended to utilize this tab also for pilot's control by connecting it to the rudder circuit. To simplify the design, however, this plan was abandoned and instead the damping rudder was connected to the control circuit with plus or minus 5 deg backlash. Thus during normal flying, with only moderate pedal operations, the control was free to act as a damping surface. For emergencies, such as spinning, this freedom would be overridden and the control would be engaged with the pedals.

* R.A.E. Report Aero. 2506, received 31st May, 1954.

Flight test results of the damping of the lateral oscillation with this damping rudder in operation are given in this report.

The variation of the efficiency of the arrangement over the range of flight conditions is analysed.

The effect of the damping rudder on aiming flight has also been investigated.

For detailed information on the theory of the damping rudder reference is made to Ref. 1.

2. *Design and Installation of the Damping Rudder.*—2.1. *Control Surface.*—The aircraft used was a standard *Vampire* Mk. 5, as illustrated in Fig. 4, but for the redesigned starboard rudder.

In order to facilitate the desired reduction of the trailing-edge angle, the rudder chord was increased and the control was given a section with flat sides tangential to the original control at the rudder hinge as shown in Fig. 6. A comparison of the plan-form of the new control with the standard surface is given in Fig. 5 together with the variation of the trailing-edge angle along the rudder span. The trailing-edge angle has been reduced from approximately 15 deg on the original rudder to 10 deg.

A balance tab was provided on the modified control the gearing of which could be varied in small steps from 0·15 : 1 up to 1 : 1. In order to increase b_1 a strip with an overall width of $\frac{3}{8}$ in. was fitted to the trailing edge over the full span of the tab.

To compensate for the increased mass moment of the new control, the geared mass was increased by 3 lb. The geometric and inertia data of the new control are given together with those of the standard rudder in Table 1.

The installation of the control is shown in Fig. 6. As a damping control the rudder must be free to move independent of the control circuit. This was assured by providing backlash corresponding to plus or minus 5 deg rudder angle within the linkage to the control circuit. In order to ease the impact when the control becomes engaged with the circuit, the bolt sliding in the slotted fork was fitted with a rubber bush. The dashpot was attached to the outside of the tail boom and covered by a fairing. The dashpot piston rod was connected to the rudder post by a lever. With the finally adopted arm of this lever of 5 in., the dashpot imposed a resistance of 50 lb ft/radn/sec to the rudder movement.

2.2. *Hydraulic Dashpot.*—The dashpot used to restrain the rudder motion was designed for operation with DTD 585, a standard mineral damping fluid. There was a by-pass through the piston (Fig. 8) which was controlled by the thermal expansion of an aluminium rod to compensate for viscosity changes over the range of temperatures 0 deg $< t <$ 100 deg F. For the present application constant damping was required down to — 60 deg F. In order to satisfy this condition the damping fluid was replaced by a synthetic oil, Silicone Dow Corning Fluid, having a substantially smaller temperature/viscosity coefficient (Fig. 7) and a freezing point well below — 60 deg F. This fluid is available for various viscosities; the grade chosen (Silicone 20 centistokes) had a viscosity at room temperature nearly identical to that of DTD 585. With Silicone the temperature compensation device produced over-compensation. This is reflected in unsystematic changes in the operational effectiveness of the damping rudder with altitude in earlier flight tests, as can be seen in Fig. 3. To meet these shortcomings the expansion rod, made originally of aluminium (Fig. 8) was replaced by one made of brass. This material has a smaller coefficient of expansion ($9{\cdot}57 \times 10^{-6}$ per unit of length per degree Fahrenheit against $12{\cdot}34 \times 10^{-6}$ for aluminium) which proved just adequate to maintain the resistance of the damper constant at 280 (lb sec ft^{-1}) over the full temperature range — 60 deg $< t <$ 100 deg F.

During earlier flights, the synthetic damping fluid was found to deteriorate in use resulting in inadequate lubrication of the dashpot cylinder. This did not occur during the present tests; most probably due to the lower air temperatures during the period of the present tests which were made during Winter and early Spring.

3. *Instrumentation.*—The recording equipment consisted of an automatic observer recording the dial readings of:

(*a*) 1 rate of yaw desyn

(*b*) 1 rudder position desyn indicator

(*c*) airspeed indicator

(*d*) altimeter

on 16 mm film. For the evaluation of aiming flights the aiming errors were recorded by a 16 mm Siemens camera installed in the nose of the fuselage.

4. *Adjustment Flights.*—A number of flights were first made to determine optimum adjustments for the gearing of the balance tab and the amount of damping to be provided by the dashpot.

The efficiency of the rudder as a yaw damper is proportional to the ratio of b_1/b_2, *i.e.*, to the trailing motion of the control. The balance tab was therefore geared to give the minimum permissible b_2 short of overbalance. This condition was obtained with a gearing tab to rudder of 0·7 : 1, which was retained during subsequent flights.

In Ref. 1 it is shown that for a given amount of rudder damping, the rudder motion responds to the aircraft oscillation with a lag progressively increasing as the aircraft speed decreases. For a given speed, rudder lag also increases with increasing rudder damping. It has been proved in Ref. 1 that optimum aircraft damping is obtained when the rudder lags the aircraft motion by approximately 45 deg. The speed at which this condition occurs, V_{SET}, is related to the amount of rudder damping, $\partial H/\partial \dot{\zeta}$ by

$$V_i = V_{\text{SET}} = \left(\frac{\partial H}{\partial \dot{\zeta}}\right) \frac{2\pi}{T_\psi V_i} \frac{2}{\rho_0 b_2 S_R C_R} . \qquad \text{(1)}$$

Above and below this speed, the efficiency of the damping rudder will drop.

With the *Vampire* Mk. 5 the damping of the lateral oscillation increases markedly at high indicated speeds (*see* Fig. 1). Thus improvements appear more desirable for medium and low speeds, in particular for flight at high altitudes. Consequently the damper was set to give optimum rudder response at $V_i = V_{\text{SET}} = 250$ m.p.h. This was achieved with the damper operating on a 5-in. arm, thus providing $\partial H/\partial \dot{\zeta} = 0{\cdot}87$ lb ft/deg/sec. The determination of the optimum damper setting is assisted by plotting the response of the rudder to aircraft yaw during lateral oscillations of the aircraft. This is illustrated for an idealised case where the hinge moment derivatives of the rudder are assumed to be constant with $b_1/b_2 = 0{\cdot}75$ in Fig. 9. The vector loci of ζ/ψ describe a semi-circle over the base which represents steady rudder trailing, *i.e.*,

$$\zeta/\psi = -\, b_1/b_2 . \qquad \text{(2)}$$

The contribution of the rudder motion to the damping of the aircraft oscillation is proportional to the component of ζ in phase with rate of yaw of aircraft motion, $\dot{\psi}$. The phase of $\dot{\psi}$ is approximately 90 deg in advance of that of ψ. Thus the component of the rudder motion utilized for aircraft damping, $\zeta_{\dot{\psi}}$, is the vertical component of the ζ vector in Fig. 9. In Ref. 1, the effect of this on the yaw damping of the aircraft oscillation has been derived as:

$$\Delta n_r = n_\zeta(\zeta_{\dot{\psi}}/\psi) \frac{T_\psi V_i}{b\pi} \frac{1}{\sqrt{\sigma}} . \qquad \text{(3)}$$

Since the indicated wavelength, $T_\psi V_i$, of the lateral oscillation is generally constant over the speed range (Fig. 21) Δn_r will vary mainly with $(\zeta_{\dot{\psi}}/\psi)$ and height. Since the logarithmic decrement δ is related to n_r by:

$$\Delta\delta = -\frac{\Delta n_r}{i_c} \sqrt{\sigma} \frac{T_\psi V_i}{2\pi} \frac{\rho_0 g}{W/S} , \qquad \text{(4)}$$

the increment in δ resulting from a given rudder response should be independent of height:

$$\Delta\delta = -\frac{1}{2\pi} \frac{n_\zeta}{i_c} \left(\frac{\zeta}{\psi}\right)_{\dot{\psi}} \frac{\rho_0 g}{W/S} \frac{(T_\psi V_i)^2}{b} . \qquad \text{(5)}$$

The actual response of the damping rudder on the *Vampire* as obtained in flight is shown in Fig. 10. The deformations of the vector loci graphs from the ideal semi-circle indicate variations in the rudder hinge-moment coefficients but it is seen that the setting adopted is a reasonable compromise over the operational range of flight conditions, as for all heights (except 40,000 ft), the optimum rudder response, *i.e.*, maximum rudder vector in counterphase to $\dot{\psi}$ occurs within the speed range.

5. *Flight Results.*—5.1. *Rudder Hinge-Moment Characteristics.*—In order to investigate the rudder trailing characteristics affecting the rudder response (Fig. 10), a number of flights were made with the damping rudder unrestrained in order to measure its free floating characteristics using equation (2):

$$b_1/b_2 \simeq -\zeta/\psi .$$

Results obtained with this techinque for b_1/b_2 of the redesigned damping rudder with geared tab are plotted in Fig. 11. For comparison, the corresponding values for the standard *Vampire* rudder are shown in Fig. 12. It is seen that b_1/b_2 has been considerably increased with the new control. In both cases, however, b_1/b_2 varies considerably over the speed range of the aircraft. With the modified control lay-out, this is mainly due to the high degree of tab balance, so that minor variations in tab effectiveness and in the b_2 of the plain rudder produce disproportionately large changes in the trailing characteristics of the complete control.

5.2. *Lateral Oscillations.*—Lateral oscillations with the tab and dashpot at their final setting were recorded over the full range of flight conditions. Examples of such records are shown in Figs. 13 to 15 and are compared in each case with recordings of the motion of the standard aircraft.

The aircraft damping has been computed in terms of the logarithmic decrement, δ, and results are plotted against V_i for four different altitudes in Figs. 16 to 19. Corresponding results with the standard aircraft and with one of the original rudders adapted as a damping control are given for comparison in each case. It can be seen that the aircraft damping is increased by a considerable amount when the damping rudder is operating. Thus the installation of the new control surface has largely fulfilled its aim, though there is still a drop in efficiency towards the higher Mach numbers. Even at the highest altitudes the requirements of AP 970 ($\delta \geqslant 0{\cdot}693$) *i.e.*, damping to half amplitude within one period of the oscillation, are, however, met over the full speed range. Over most of the range of flight condition the damping of the lateral oscillation is actually twice this value.

The period of the lateral oscillation, T_ψ, has not changed with the new control installed, apart from the high-speed range (Fig. 20) where the period is increased when compared with the standard aircraft with fixed rudders. The same trend is represented in Fig. 21 where the indicated wavelength ($T_\psi V_i$) of the lateral oscillation is plotted.

For an assessment of the contribution of the damping rudder and its variation over the range of flight conditions, the increment $\Delta\delta$ in the logarithmic decrement of the lateral oscillation has been computed as:

$$\Delta\delta = [\delta]_{\text{Rudder operating}} - [\delta]_{\text{Rudders fixed}} . \qquad (6)$$

Results are plotted in Fig. 22 against V_i and in Fig. 23 against Mach number.

It has been shown in Ref. 1 that the damping rudder will produce an increment in δ which will vary over the speed range as:

$$\frac{(\Delta\delta)_{V_i}}{(\Delta\delta)_{V_i = V_{\text{SET}}}} = 2\,\frac{V_i/V_{\text{SET}}}{1 + (V_i/V_{\text{SET}})^2}\,\frac{(b_1/b_2)_{V_i}}{(b_1/b_2)_{V_{\text{SET}}}}, \qquad (7)$$

if the wavelength, $T_\psi V_i$, is constant. Thus, if the rudder hinge-moment derivatives were constant, $\Delta\delta$ would vary with V_i, according to the first term in equation (7). This is represented in Fig. 24.

Assuming that the damper is set to give optimum rudder response at $V_{SET} = 250$ m.p.h., the corresponding speed range covered during the flight tests on the *Vampire*, $175 < V_i < 450$ m.p.h., is marked on this diagram. It is seen that the theoretical variation of $\Delta\delta$ due to speed alone is very moderate over this range. The large variations recorded in flight (Figs. 22 and 23) must therefore be attributed mainly to changes in b_1 and b_2 with both V_i and Mach number, as discussed earlier in this report and illustrated in Fig. 11.

5.4. *Aiming Flights.*—In order to assess one of the practical implications of the improvement in aircraft damping achieved, aiming flights were made using both air and ground targets. The aiming errors were recorded by a camera in the nose of the aircraft and computed as the angular deviation of the sighting line (fixed gun-sight) from the target.

For air to air aiming the target aircraft was instructed to fly a straight course. No noticeable turbulence was met during these flights. In the absence of any natural disturbances under these idealized conditions the *Vampire* sight line was initially displaced by approximately half of the semi-span off the target centre. After recording had commenced the pilot tried to resight into the target centre, *i.e.*, the fuselage of the target aircraft.

For air to ground aiming the top of a tower was used as a target and no special instructions were given to the pilots. These flights were made during various degrees of air turbulence.

Typical examples of aiming runs air to air are given in Figs. 25 to 26. In each case corresponding records obtained by the same pilot with the standard aircraft are added for comparison. The reduction of the aim wander with the damping rudder operating is apparent with both pilots, though each applies a different technique.

In aiming at ground targets, no conspicuous improvement was recorded with the damping rudder and it was impossible to select runs made at comparable atmospheric conditions.

The acheivements and also the general appraisal varied considerably between individual pilots. The results of such tests reflect, of course, not only the characteristics of the aircraft but also pilots' skill and in particular familiarization with these characteristics. There was apparently not enough time for full familiarization and the results have suffered in consequence.

When compared with the standard aircraft, the modified aircraft will be different mainly in two aspects, apart from the primarily intended improved damping in yaw:

(*a*) Reduced weathercock stability due to the exaggerated rudder trailing motion

(*b*) The rudder power is halved for a given pedal movement within the range of small deflections, whereby, however, the original correlation between pedal force and control power is maintained.

Pilots' complaints were in fact mainly on directional control, either criticising a tendency for the aircraft to sideslip or poor rudder response. This would confirm the widely held view that control predominantly by force is preferable to control by movement.

The majority of pilots, however, considered the damping rudder a considerable assistance for aiming, particularly at the higher altitudes where the basic aircraft is poorly damped.

6. *Conclusions.*—With the modified damping rudder at its final setting the damping of the lateral oscillations of the *Vampire* Mk. 5 was increased by an increment in δ varying between $1 \cdot 1$ and $0 \cdot 4$ over the range of flight conditions. The larger value was actually maintained over the greater part of the speed range. At higher Mach numbers, however, changes in the tab and rudder hinge-moment derivatives resulted in a drop to the lower value. This gain in aircraft damping amounted to several times the damping of the standard aircraft, particularly at higher altitudes, and it was generally more than twice the gain achieved previously when a standard rudder was used as the damping surface.

The hydraulic dashpot used to restrain the motion of the damping rudder operated very satisfactorily using Silicone damping fluid. After modifications to the temperature-compensation mechanism, the dashpot provided practically constant damping over the full range of atmospheric temperatures met with in flight.

In order to achieve maximum rudder floating, the balance tab was geared to the damping rudder very close to the limit of overbalance. The resulting rudder trailing reduced the weather-cock stability of the aircraft ; this was criticized by some pilots as it did apparently impair the realization of the full benefit from the improved aircraft damping in aiming flights. However, with the majority of pilots the accuracy of air to air aiming was considerably improved with the damping rudder operating.

It may be concluded that a better compromise in the aircraft handling characteristics might have been achieved with a lesser degree of rudder floating even if the gain in yaw damping were thereby reduced.

LIST OF SYMBOLS

b		Wing span
b_1	=	$-(\partial C_H/\partial\beta)$ rudder floating derivative
b_2	=	$\partial C_H/\partial\zeta$ rudder restoring derivative
C_H		Rudder hinge-moment coefficient
C_R		Rudder mean chord
C_T		Tab mean chord
g		Gravitational acceleration
H		Rudder hinge moment
i_c		Inertia coefficient in yaw
l_F		Fin arm from c.g.
n_r		Aircraft damping in yaw derivative
S		Wing area
S_R		Rudder area } aft of hinge
S_T		Tab area } aft of hinge
T_ψ		Period } of the lateral oscillation
$(T_\psi V_i)$		Indicated wavelengths } of the lateral oscillation
V_i		Indicated airspeed
V_{SET}		Indicated speed for optimum rudder damping
W		Weight of aircraft
W_R		Rudder weight
x_R		Distance of rudder c.g. from rudder hinge
β		Angle of sideslip
δ		Logarithmic decrement of the lateral oscillation
$\Delta\delta$		Increment in δ due to operation of damping rudder
ζ		Rudder angle
ψ		Angle of yaw
$\Delta\psi$		Aiming error

REFERENCE

No.	*Author*	*Title, etc.*
1	W. Pinsker	Control surfaces restrained by viscous friction as a means of damping aircraft oscillations. R. & M. 2962. February, 1953.

TABLE 1

Geometric and Inertia Data of the Vampire Mk. 5

Aircraft

$W = 8{,}400$ lb weight

$S = 262$ ft² wing area

$b = 38$ ft wing span

$l_F = 17{\cdot}0$ ft fin arm

Standard rudder	New rudder	
$S_R = 3{\cdot}323$ ft²	$4{\cdot}075$ ft²	area aft of hinge
$C_R = 1{\cdot}34$ ft	$1{\cdot}621$ ft²	mean chord
$b_R = 2{\cdot}48$ ft	$2{\cdot}514$ ft	span
$S_T = 0{\cdot}069$ ft²*	$0{\cdot}488$ ft²	tab area
$C_T = 0{\cdot}115$ ft	$0{\cdot}25$ ft	tab mean chord
$W_R = 21$ lb	$27{\cdot}1$ lb	rudder weight including mass balance and tab
$\theta = 5{\cdot}27$ lb ft²	$7{\cdot}64$ lb ft²	rudder inertia
$x_R = -0{\cdot}075$ ft	$-0{\cdot}06$ ft	rudder c.g. in front of hinge axis

* Trim tab.

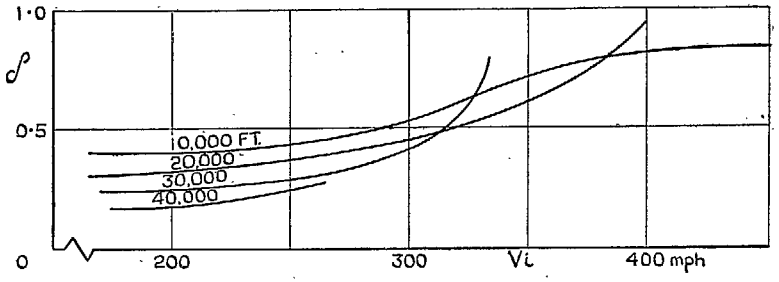

FIG. 1. Logarithmic decrement δ of the lateral oscillation of the standard *Vampire* Mk. 5 with fixed controls.

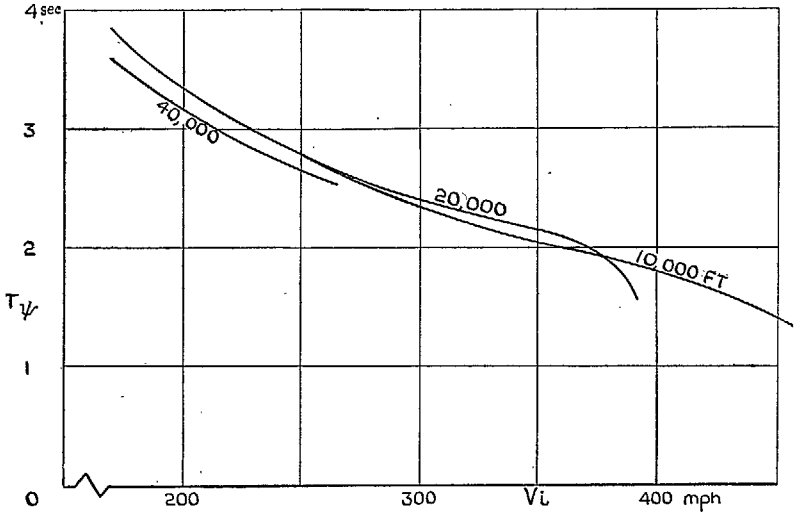

FIG. 2. Period T_ψ of the lateral oscillation of the standard *Vampire* Mk. 5 with fixed controls.

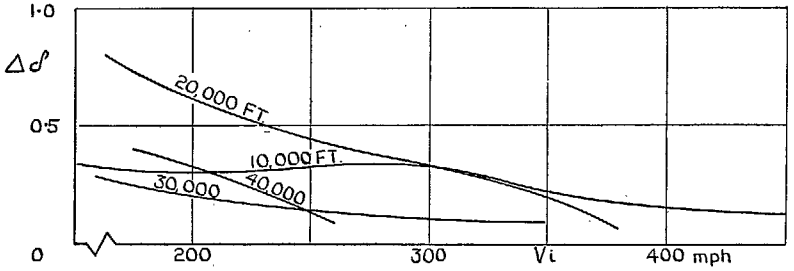

FIG. 3. Increment in the logarithmic decrement of the *Vampire* due to the operation of one rudder as damping control.

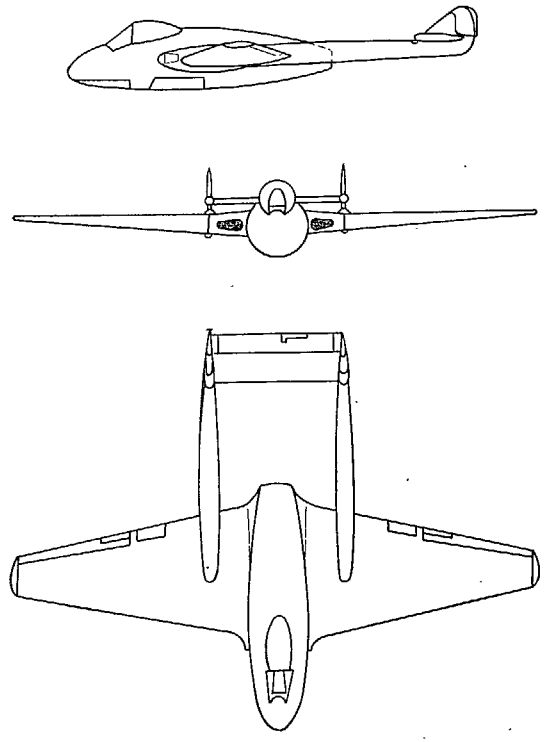

FIG. 4. G.A. of the *Vampire* Mk. 5 with modified starboard rudder.

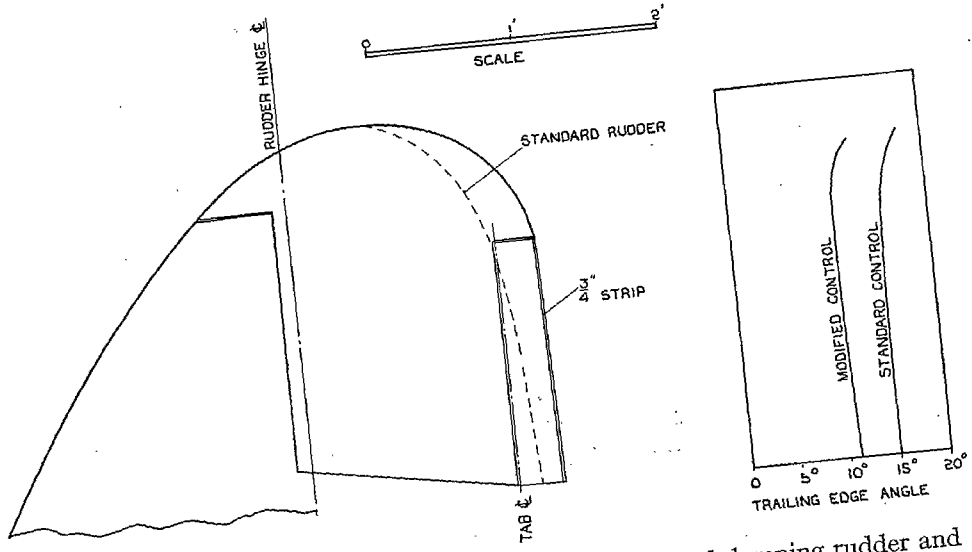

FIG. 5. Plan-form and trailing-edge angle of the modified damping rudder and standard rudder.

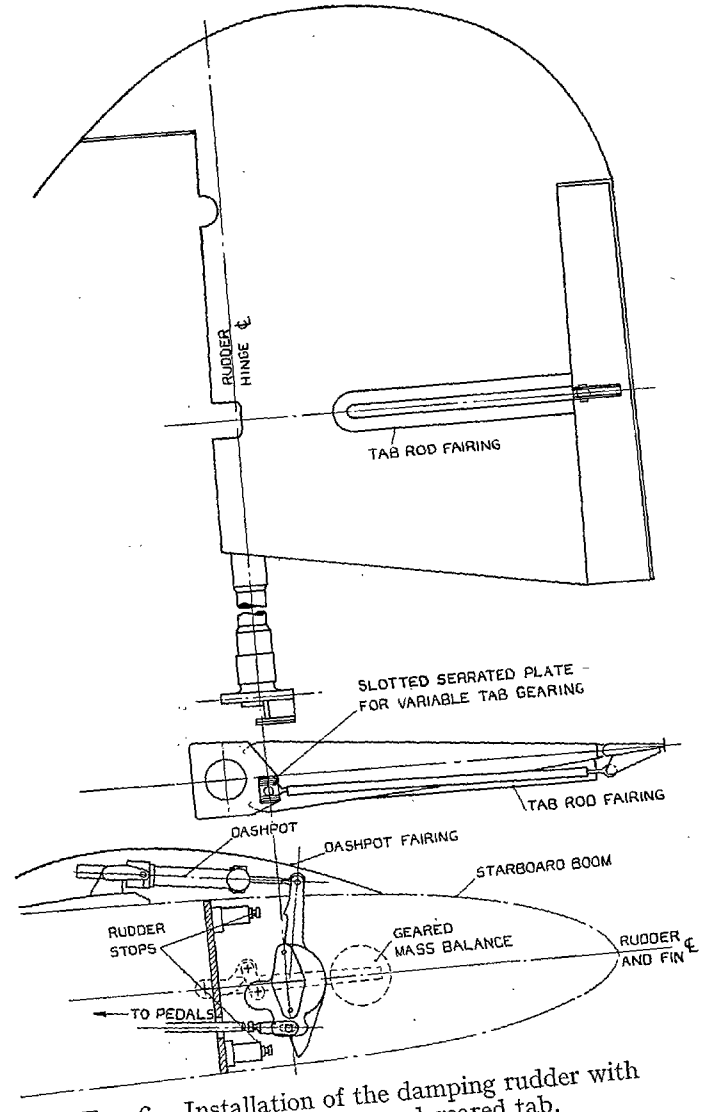

FIG. 6. Installation of the damping rudder with hydraulic dashpot and geared tab.

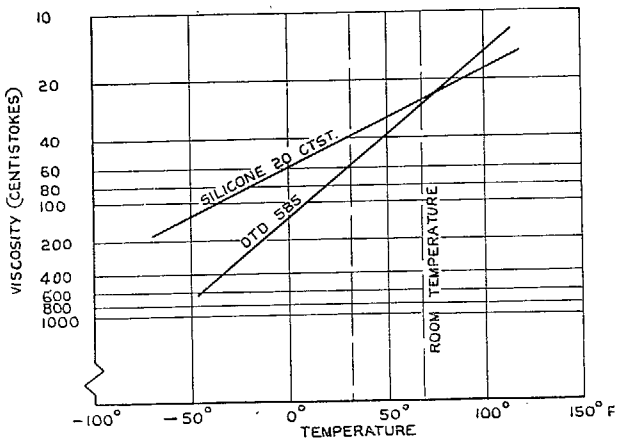

FIG. 7. Change of viscosity with temperature of Silicone Dow Corning Fluid, 20 centistokes, and DTD 585.

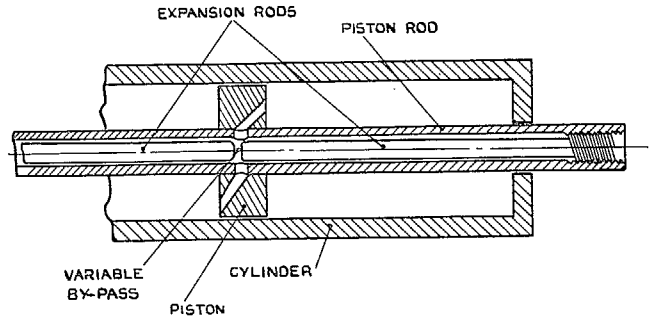

FIG. 8. Diagram of the dashpot with temperature compensation.

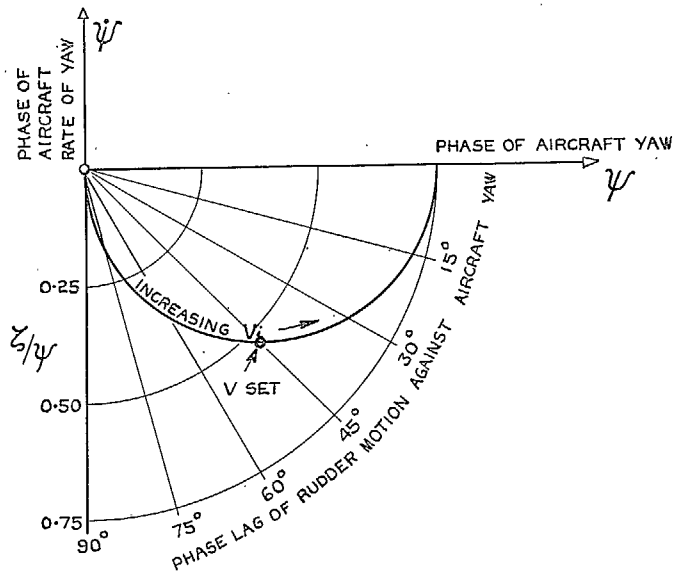

FIG. 9. Theoretical response of a damping rudder with constant hinge-moment derivatives to the lateral oscillation of an aircraft.

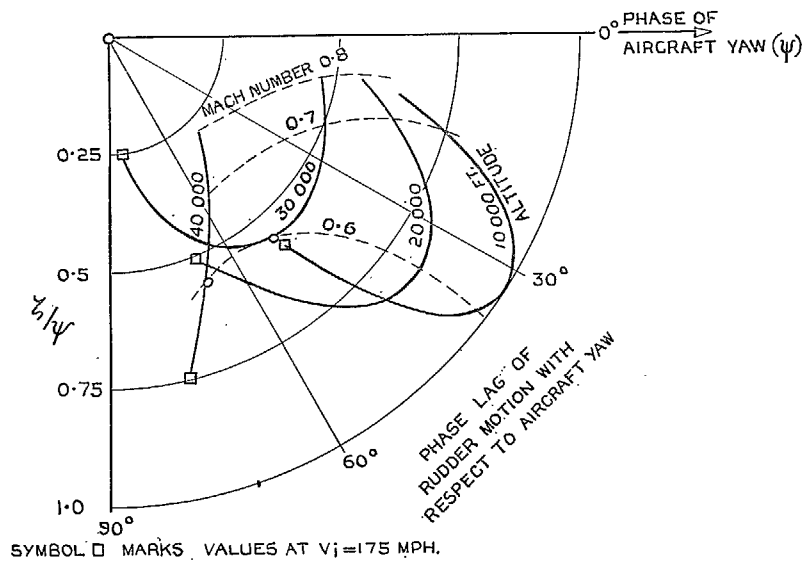

FIG. 10. Response of the damping rudder to the lateral oscillation of the *Vampire*.

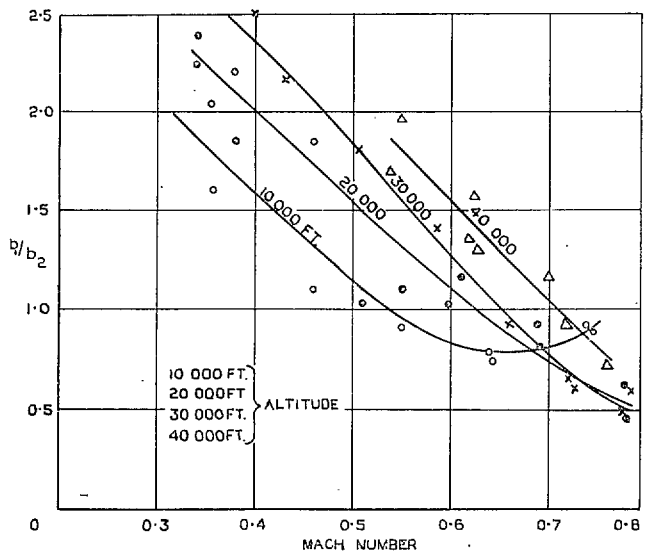

FIG. 11. Rudder floating characteristics of the redesigned control surface with balance tab.

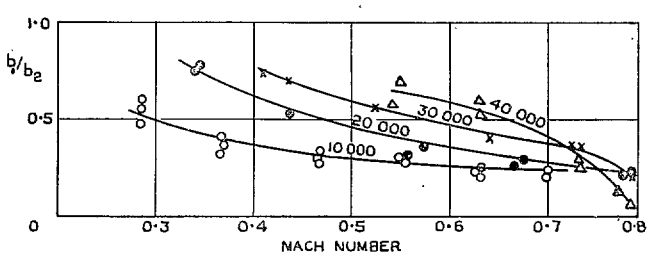

FIG. 12. Floating characteristics of the standard *Vampire* rudder.

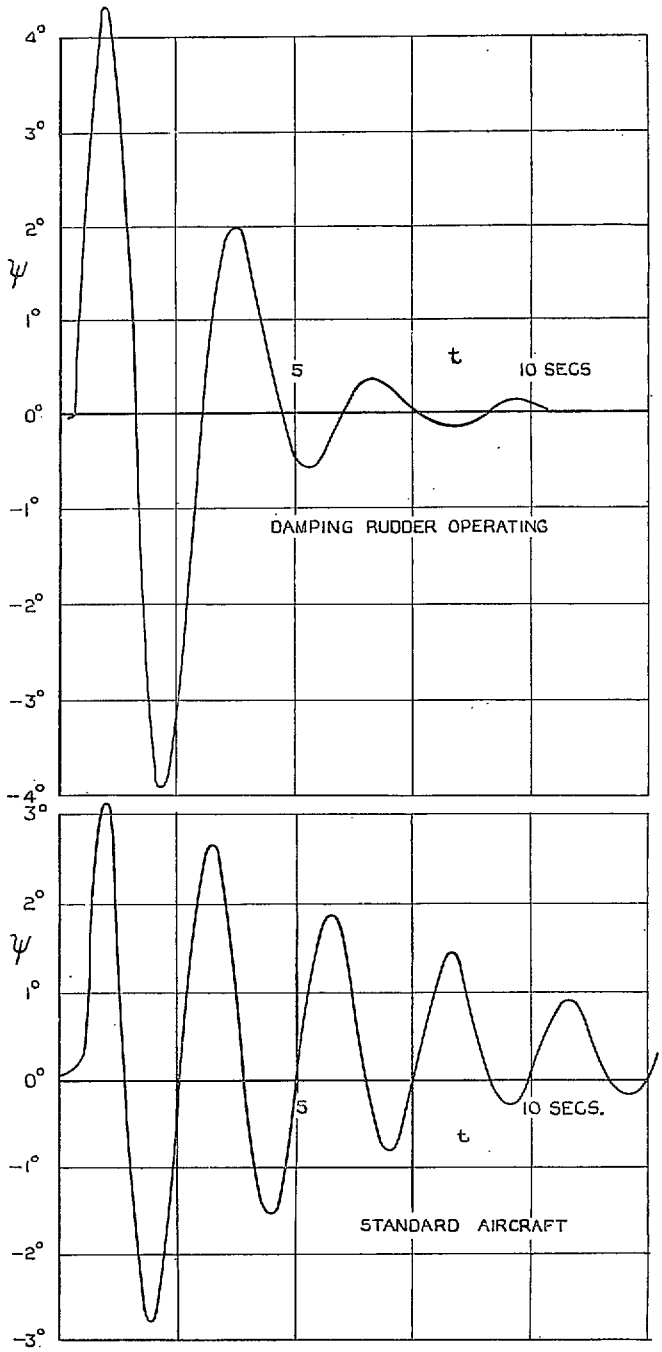

FIG. 13. Flight records of the lateral oscillation of the *Vampire* Mk. 5 with and without the damping rudder operating at $V_i = 290$ m.p.h. and 10,000 ft altitude.

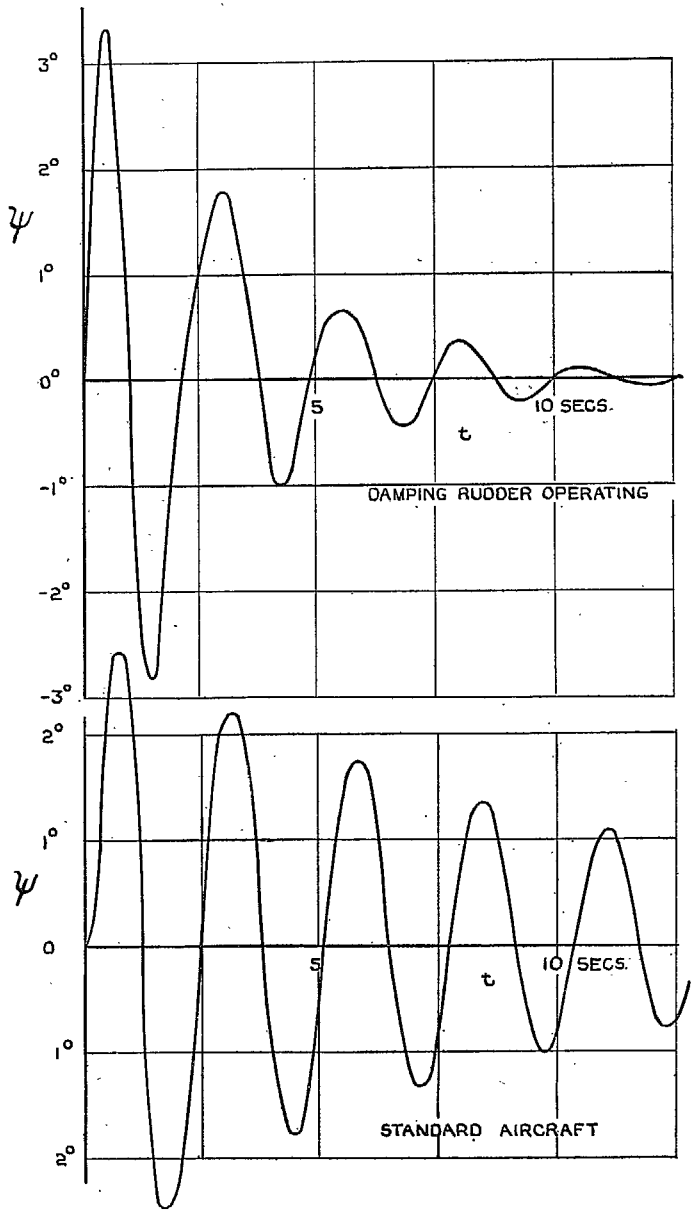

FIG. 14. Flight records of the lateral oscillation of the *Vampire* Mk. 5 with and without the damping rudder operating at $V_i = 280$ m.p.h. and 30,000 ft altitude.

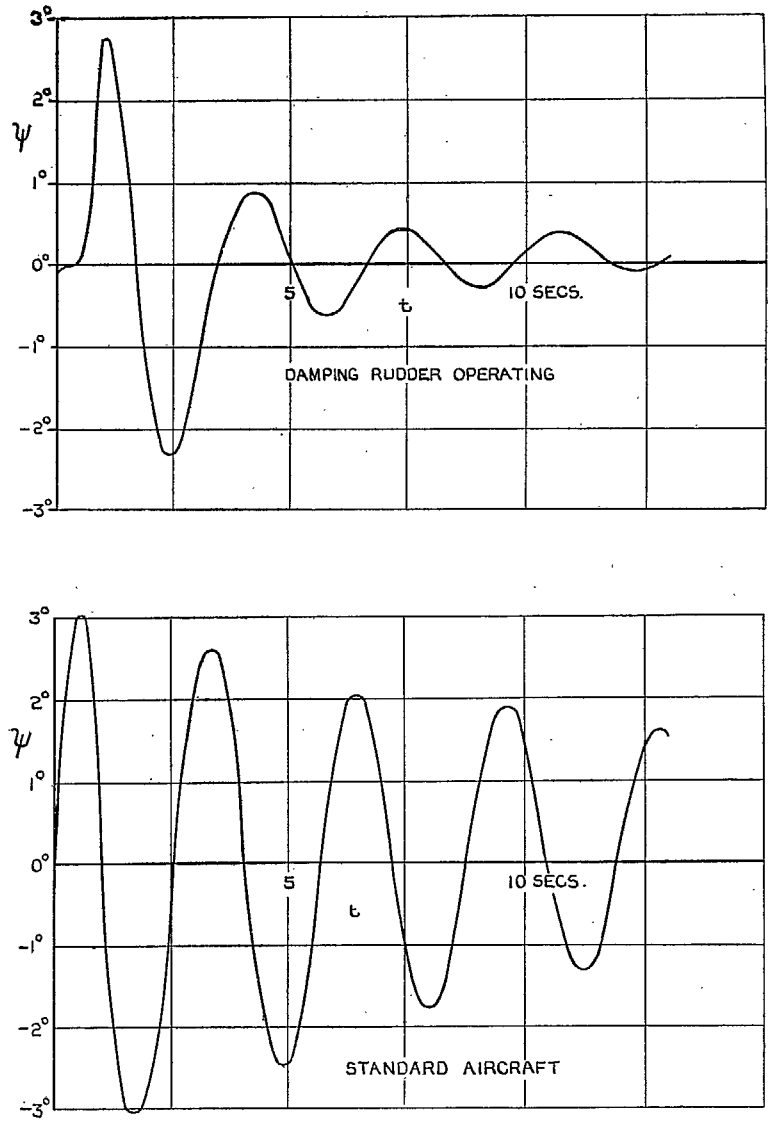

FIG. 15. Flight records of the lateral oscillation of the *Vampire* Mk. 5 with and without the damping rudder operating at $V_i = 203$ m.p.h. and 40,000 ft altitude.

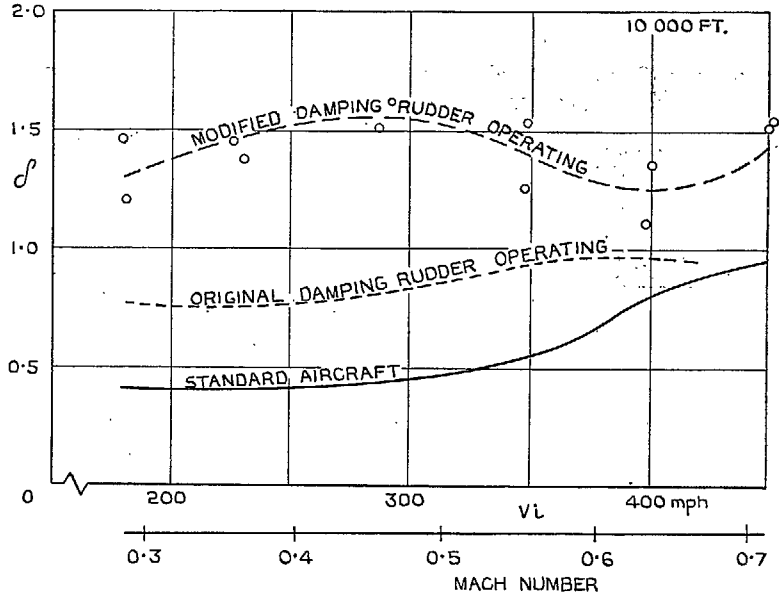

FIG. 16. Logarithmic decrement δ of the lateral oscillation of the *Vampire* Mk. 5 with and without damping rudder at 10,000 ft altitude.

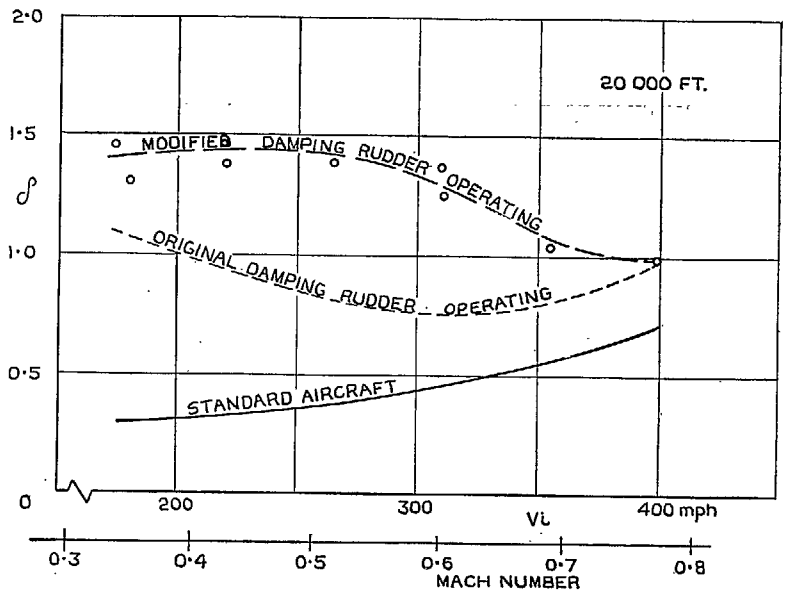

FIG. 17. Logarithmic decrement δ of the lateral oscillation of the *Vampire* Mk. 5 with and without damping rudder at 20,000 ft altitude.

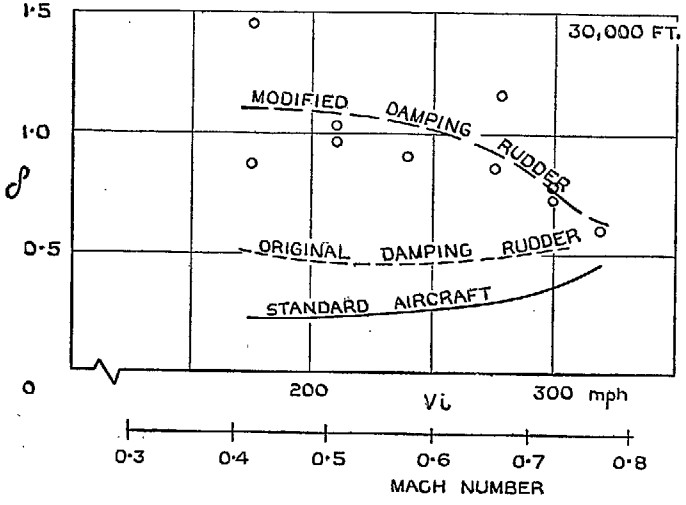

FIG. 18. Logarithmic decrement δ of the lateral oscillation of the *Vampire* Mk. 5 with and without damping rudder at 30,000 ft altitude.

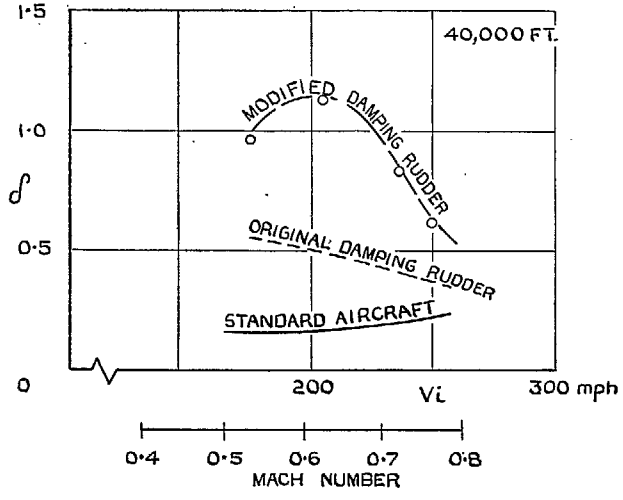

FIG. 19. Logarithmic decrement δ of the lateral oscillation of the *Vampire* Mk. 5 with and without damping rudder at 40,000 ft altitude.

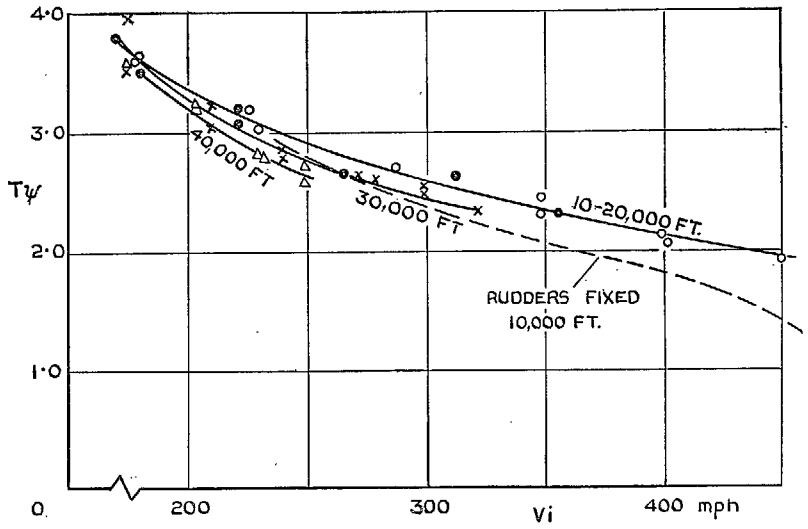

FIG. 20. Period T_ψ of the lateral oscillation of the *Vampire* Mk. 5 with and without damping rudder.

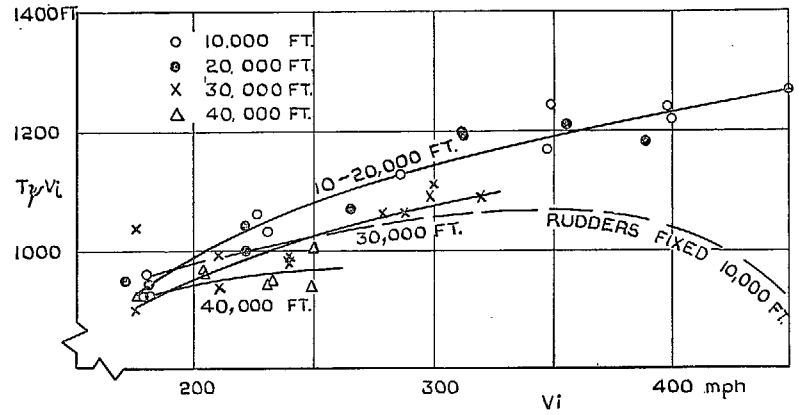

FIG. 21. Indicated wavelength $T_\psi V_i$ of the *Vampire* Mk. 5 with and without damping rudder.

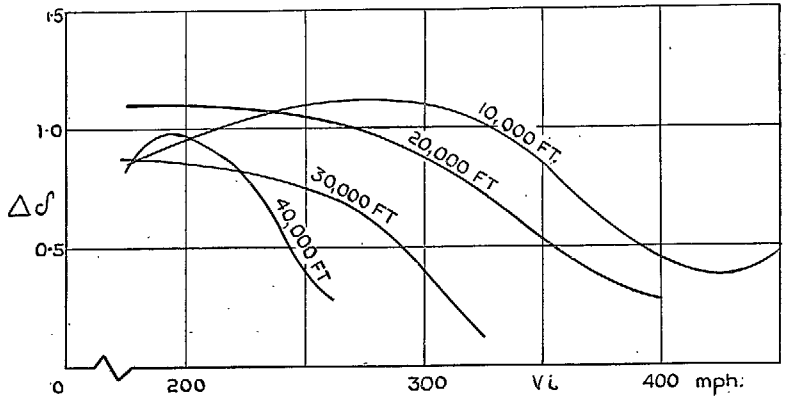

FIG. 22. Increment in the logarithmic decrement of the lateral oscillation of the *Vampire* due to the damping rudder against V_i.

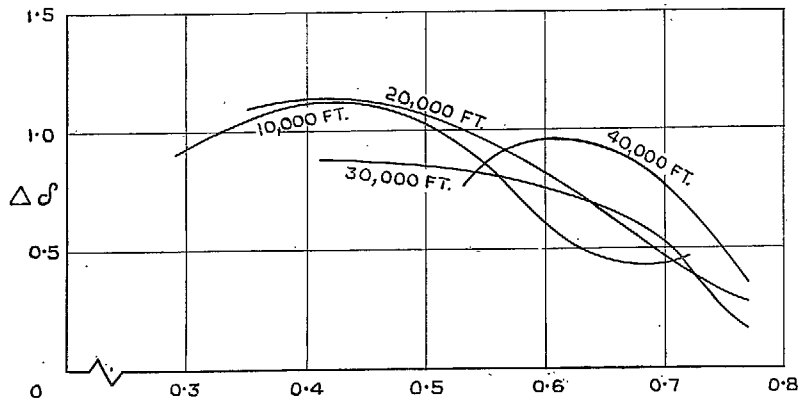

FIG. 23. Increment in δ against Mach number.

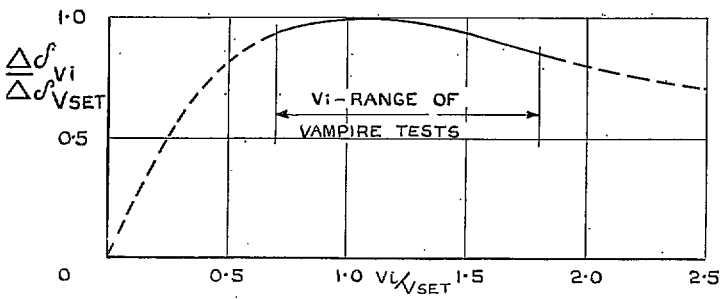

FIG. 24. Theoretical variation of $\Delta\delta$ with V_i if damper is set to give optimum rudder response at $V_i = V_{SET}$.

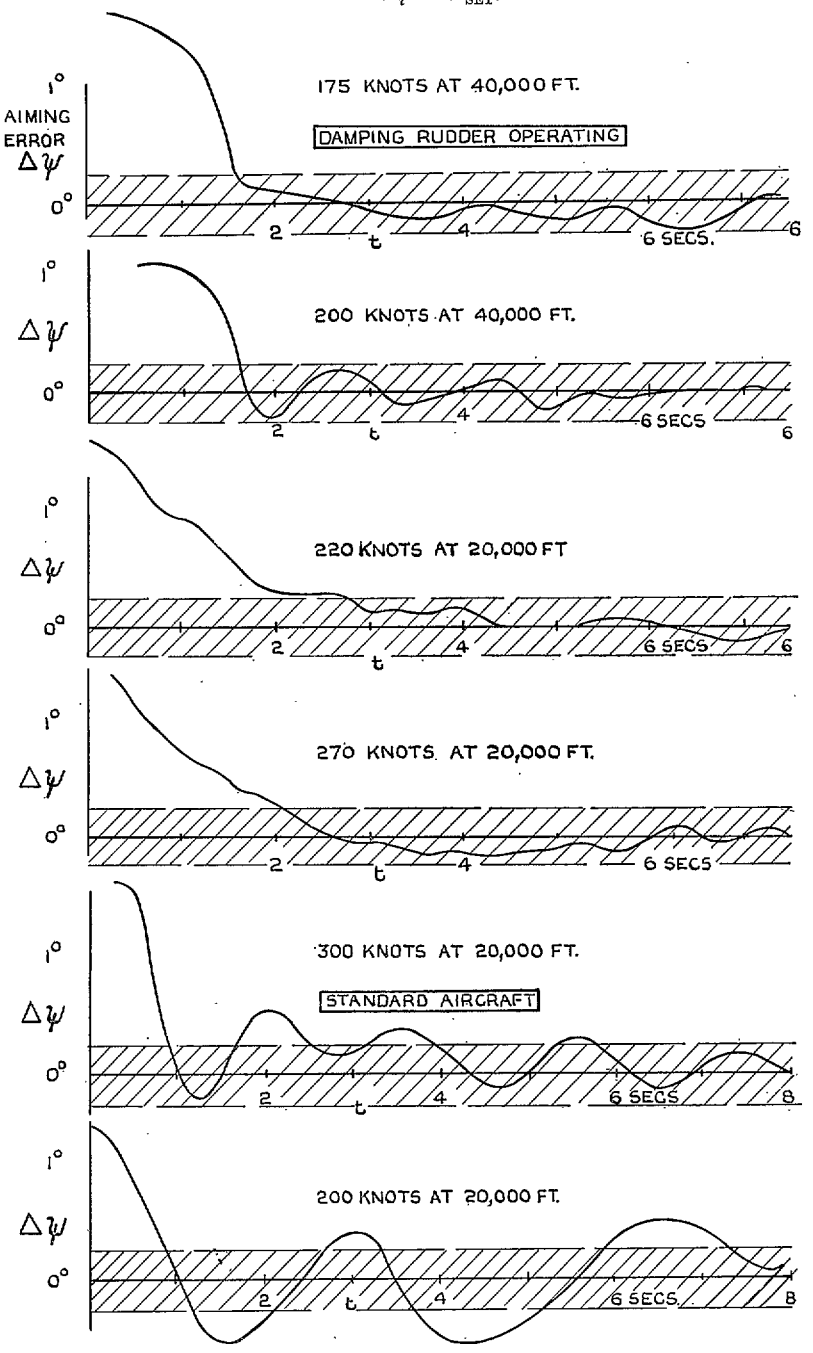

FIG. 25. Aiming air to air at 40,000 ft and 10,000 ft with and without the damping rudder operating pilot 'A'.

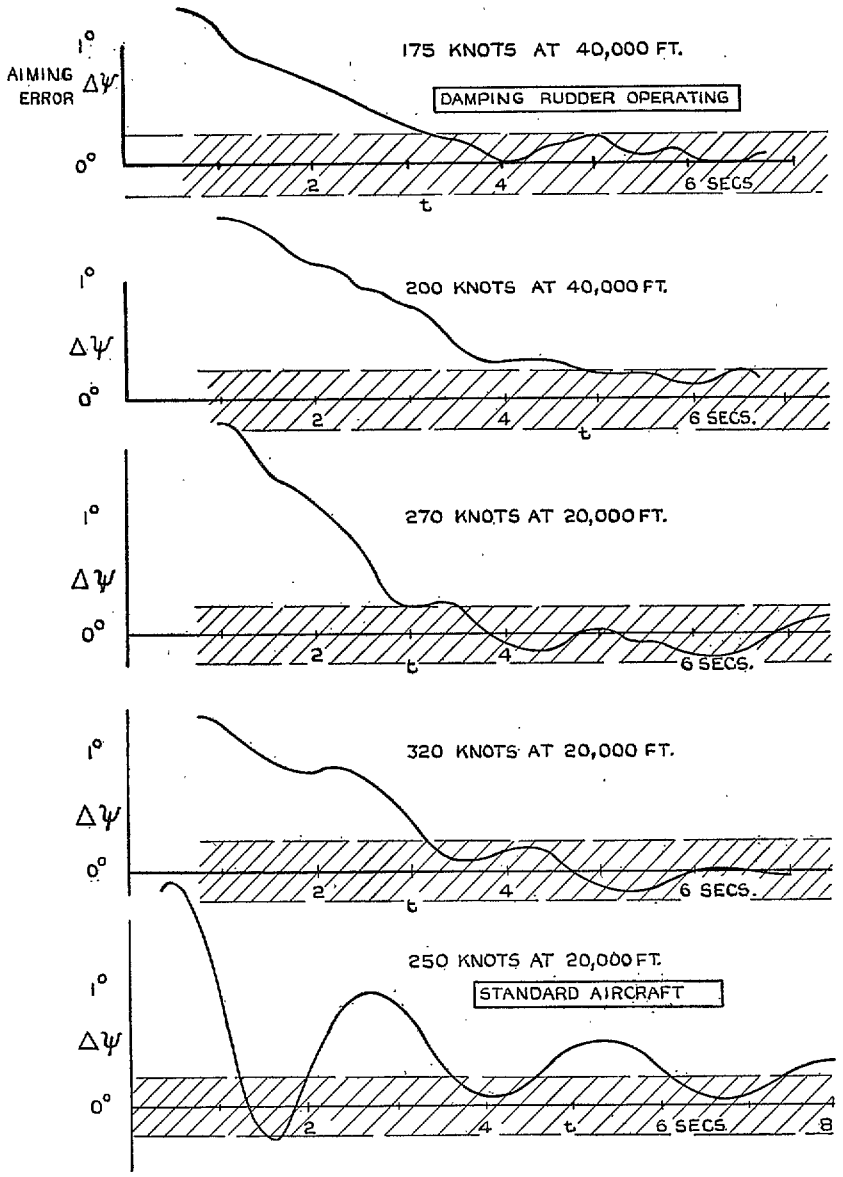

FIG. 26. Aiming air to air at 40,000 ft and 20,000 ft altitude with and without the damping rudder operating pilot 'B'.

(68096) Wt. 20/9036 K.7 11/57 Hw.

Publications of the Aeronautical Research Council

ANNUAL TECHNICAL REPORTS OF THE AERONAUTICAL RESEARCH COUNCIL (BOUND VOLUMES)

1939 Vol. I. Aerodynamics General, Performance, Airscrews, Engines. 50*s.* (51*s.* 9*d.*).
Vol. II. Stability and Control, Flutter and Vibration, Instruments, Structures, Seaplanes, etc. 63*s.* (64*s.* 9*d.*)

1940 Aero and Hydrodynamics, Aerofoils, Airscrews, Engines, Flutter, Icing, Stability and Control Structures, and a miscellaneous section. 50*s.* (51*s.* 9*d.*)

1941 Aero and Hydrodynamics, Aerofoils, Airscrews, Engines, Flutter, Stability and Control Structures. 63*s.* (64*s.* 9*d.*)

1942 Vol. I. Aero and Hydrodynamics, Aerofoils, Airscrews, Engines. 75*s.* (76*s.* 9*d.*)
Vol. II. Noise, Parachutes, Stability and Control, Structures, Vibration, Wind Tunnels. 47*s.* 6*d.* (49*s.* 3*d.*)

1943 Vol. I. Aerodynamics, Aerofoils, Airscrews. 80*s.* (81*s.* 9*d.*)
Vol. II. Engines, Flutter, Materials, Parachutes, Performance, Stability and Control, Structures. 90*s.* (92*s.* 6*d.*)

1944 Vol. I. Aero and Hydrodynamics, Aerofoils, Aircraft, Airscrews, Controls. 84*s.* (86*s.* 3*d.*)
Vol. II. Flutter and Vibration, Materials, Miscellaneous, Navigation, Parachutes, Performance, Plates and Panels, Stability, Structures, Test Equipment, Wind Tunnels. 84*s.* (86*s.* 3*d.*)

1945 Vol. I. Aero and Hydrodynamics, Aerofoils. 130*s.* (132*s.* 6*d.*)
Vol. II. Aircraft, Airscrews, Controls. 130*s.* (132*s.* 6*d.*)
Vol. III. Flutter and Vibration, Instruments, Miscellaneous, Parachutes, Plates and Panels, Propulsion. 130*s.* (132*s.* 3*d.*)
Vol. IV. Stability, Structures, Wind Tunnels, Wind Tunnel Technique. 130*s.* (132*s.* 3*d.*)

Annual Reports of the Aeronautical Research Council—

1937 2*s.* (2*s.* 2*d.*) 1938 1*s.* 6*d.* (1*s.* 8*d.*) 1939–48 3*s.* (3*s.* 3*d.*)

Index to all Reports and Memoranda published in the Annual Technical Reports, and separately—

April, 1950 - - - - R. & M. 2600 2*s.* 6*d.* (2*s.* 8*d.*)

Author Index to all Reports and Memoranda of the Aeronautical Research Council—

1909—January, 1954 R. & M. No. 2570 15*s.* (15*s.* 6*d.*)

Indexes to the Technical Reports of the Aeronautical Research Council—

December 1, 1936—June 30, 1939	R. & M. No. 1850	1*s.* 3*d.* (1*s.* 5*d.*)
July 1, 1939—June 30, 1945	R. & M. No. 1950	1*s.* (1*s.* 2*d.*)
July 1, 1945—June 30, 1946	R. & M. No. 2050	1*s.* (1*s.* 2*d.*)
July 1, 1946—December 31, 1946	R. & M. No. 2150	1*s.* 3*d.* (1*s.* 5*d.*)
January 1, 1947—June 30, 1947	R. & M. No. 2250	1*s.* 3*d.* (1*s.* 5*d.*)

Published Reports and Memoranda of the Aeronautical Research Council—

Between Nos. 2251–2349	R. & M. No. 2350	1*s.* 9*d.* (1*s.* 11*d.*)
Between Nos. 2351–2449	R. & M. No. 2450	2*s.* (2*s.* 2*d.*)
Between Nos. 2451–2549	R. & M. No. 2550	2*s.* 6*d.* (2*s.* 8*d.*)
Between Nos. 2551–2649	R. & M. No. 2650	2*s.* 6*d.* (2*s.* 8*d.*)

Prices in brackets include postage

HER MAJESTY'S STATIONERY OFFICE

York House, Kingsway, London, W.C.2; 423 Oxford Street, London, W.1; 13a Castle Street, Edinburgh 2; 39 King Street, Manchester 2; 2 Edmund Street, Birmingham 3; 109 St. Mary Street, Cardiff; Tower Lane, Bristol 1; 80 Chichester Street, Belfast, *or through any bookseller.*

S.O. Code No. 23-3014